Disordered purification phase transition in hybrid random circuits

Kengo Anzai,[1,2] Hiroaki Matsueda,[2,3] and Yoshihito Kuno[4]
[1]*Faculty of Science and Engineering, Akita University, Akita 010-8502, Japan*
[2]*Department of Applied Physics, Graduate School of Engineering, Tohoku University, Sendai 980-8579, Japan*
[3]*Center for Science and Innovation in Spintronics, Tohoku University, Sendai 980-8577, Japan*
[4]*Graduate School of Engineering Science, Akita University, Akita 010-8502, Japan*

(Received 25 July 2025; revised 29 October 2025; accepted 5 December 2025; published 20 January 2026)

Noise is inevitable in realistic quantum circuits. It arises randomly in space. Inspired by the spatial nonuniformity of the noise, we investigate the effects of spatial modulation on quantum phase transitions in a hybrid random Clifford circuit with a mixed initial state. As an efficient observable for extracting quantum entanglement in mixed states, we employ many-body negativity. The behavior of the many-body negativity well characterizes the presence of the phase transitions and its criticality. We find the effect of spatial nonuniformity in measurement probability on the phase transition. The criticality of the phase transition changes from that of uniform probability, which is elucidated by the argument of the Harris criterion. The critical correlation length exponent ν changes from $\nu < 2$ for uniform probability to $\nu > 2$ for spatially modulated probability. We further investigate a setting where a two-site random Clifford gate becomes spatially (quasi)modulated. We find that the modulation induces a phase transition, leading to a different pure phase where a short-range quantum entanglement remains.

DOI: 10.1103/mb36-pc91

I. INTRODUCTION

A measurement-induced phase transition (MIPT) is characterized by the average entanglement entropy of pure states in random quantum circuits [1–3]. The circuits are composed of local measurements and random unitary gates, and the former (latter) elements break (induce) local entanglement of the initial state. The origin of the transition is this competition of entanglement. In addition, these gate operations can be viewed as an artificial time evolution of an effective Hamiltonian. The late-time steady state of a quantum circuit is realized by the thermal equilibrium state or the ground state of the Hamiltonian. Although deriving this Hamiltonian can be challenging, previous research demonstrated that the effective Hamiltonian can be mapped onto a ferromagnetic Ising model via a replica trick for specific cases of hybrid random circuits [4–7]. In addition, a MIPT observed in these systems corresponds to the transition of two-dimensional bond percolation [1,2,8]. Thus, the study (i.e., the statistical mechanical properties of phase transitions) of MIPTs has attracted much attention.

The above-mentioned MIPT occurs for pure states. In cases of initially mixed states, a purification phase transition appears instead of the entanglement transition in MIPTs, and the nature of the purification phase transition is measured by using logarithmic purity [9]. The measurement purifies the state, and a critical measurement probability exists for the purification phase transition. Although both MIPTs and the purification phase transition are induced by measurements, they reflect different effects: Measurements break local entanglement in the former, while measurements purify the system in the latter. This difference highlights the distinct roles measurements play in the induction of phase transitions. In this sense, it is interesting to examine the entanglement structure in mixed states.

These two phase transitions are strongly affected by external noise. In general, noise on a circuit arises randomly in space. Especially, we investigate the effects of the spatial nonuniformity in a circuit on purification phase transitions. In this work, we consider its effects in projective measurements [10–12] and local two-qubit random unitaries, instead of applying a standard noise model like a local quantum channel. In this study, we employ the same quenched spatial randomness as in Ref. [10]. However, our setup differs from Ref. [10] because we focus on the mixed-state dynamics. It should also be noted that the observables we consider are different. Introducing the spatial randomness is qualitatively related to a disordered effective Hamiltonian. In statistical mechanics, the stability of critical points against disorder is evaluated using the Harris criterion [13], which focuses on the correlation length critical exponent. In particular, when disorder affects the universality class of a quantum phase transition, the critical behavior can change, potentially altering the value of the correlation length critical exponent itself. Understanding whether this phenomenon occurs even in quantum phase transitions with a mixed initial state is important. In this work, we employ many-body negativity (MBN) [14–16], which is a suitable entanglement measure in the random quantum circuit to detect the critical exponent in mixed states. Previous works

Published by the American Physical Society under the terms of the Creative Commons Attribution 4.0 International license. Further distribution of this work must maintain attribution to the author(s) and the published article's title, journal citation, and DOI.

[17,18] successfully characterized MIPTs using MBN under a subsystem partition, and those works mainly focused on pure states. However, the application to mixed states, its dynamics, and its phase transition, as well as detailed numerical observations for them, are still lacking. Furthermore, Ref. [9] discussed whether the purification phase transition and the entanglement transition coincide. Therefore, the entanglement transition in mixed states has attracted growing interest. In this work, we numerically investigate the behavior of MBN precisely. The steady state characterized by MBN sometimes shows different power-law scalings in the structure and model of the system. For example, a model in a random Clifford circuit with boundary decoherence has an $L^{1/3}$ power law [16] (where L is system size). How MBN scales in our models is curious. In this work, we find that the entanglement phase transition is captured by MBN. Moreover, we find that the criticality of the phase transitions is changed in the spatially modulated measurements. This change can be understood by the Harris criterion. This result suggests that we can also apply this criterion in quantum circuits. With respect to spatial nonuniformity in local two-qubit random unitaries, we expect localized states distinct from the one observed in the above case to emerge because the action of local two-qubit random unitaries on a few sites leads to the formation of short-range entanglement. The short-range entanglement is in contrast to the uniform case described above, where unitary gates act on all sites, leading to the formation of long-range entanglement (excluding the effect of measurements). We consider quasiperiodic modulation under unitary gates. The modulation could alter the nature of the steady state. We identified area-law-like phase, distinguishable from the pure phase by the entanglement structure of the subsystems. We also find that the effective Hamiltonian for the spatially modulated gates is given by a quasimodulated ferromagnetic ZY coupling model. These results show that the spatial modulation significantly affects the quantum phase transition.

The rest of this paper is organized as follows. In Sec. II, we introduce a random Clifford unitary circuit with on-site projective measurements and a spatial modulation for the measurement probability. In Sec. III, the physical quantities of interest are explained. There, logarithmic purity and MBN are introduced. In Sec. IV, numerical results are given. From the behaviors of MBN and logarithmic purity, the transition properties and their quantum criticality are numerically investigated in detail. In Sec. V, we provide a discussion of the numerical results obtained in Sec. IV. In particular, the effects of the spatially modulated probability on the criticality from the viewpoint of the Harris criterion are discussed. In Sec. VI, we numerically investigate the effect of the spatially modulated application of the random Clifford gate with a certain uniform measurement probability for this mixed-state dynamics. Section VII is devoted to the conclusion.

II. RANDOM CLIFFORD CIRCUIT WITH SPATIALLY MODULATED MEASUREMENT PROBABILITY

We consider a one-dimensional system of L qubits with periodic boundary conditions and study hybrid random Clifford circuits [1,2,9] (see Fig. 1). The circuits consist of two parts: The first one is a two-site random unitary layer, where

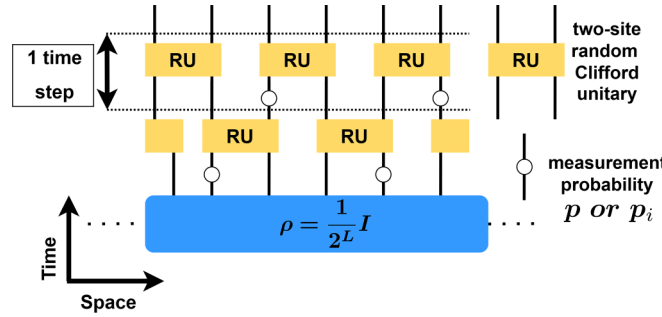


FIG. 1. A schematic illustration of the hybrid random Clifford circuit. The yellow blocks represent two-site random Clifford unitary gates, and the small white circles represent projective measurements of the on-site Z_i measurement operator with measurement rate p or p_i. One time step consists of one measurement layer and a layer of two-site random Clifford unitaries, where the unitary gates do not overlap.

the two-site gate is picked up from the Clifford group [19,20] randomly, and the second one is a measurement layer where each site is measured by a projective measurement of the on-site Z_i measurement operator with a uniform measurement probability p or a *site-dependent* measurement probability p_i, where i is the site number ($i = 0, 1, \ldots, L-1$). We employ a spatially modulated probability given by $p_i \equiv w_i^n$, where w_i is a uniform random value in [0, 1] and n controls the average probability for the entire system given by $\bar{p} = 1/(n+1)$ [10]. The circuit with $\bar{p} = 1/(n+1)$ can be compared with the uniform probability case studied previously [9]. One time step is defined as a pair consisting of a unitary layer followed by a measurement layer. In the unitary layer, local two-qubit unitaries act on neighboring pairs of qubits. Each unitary layer has $L/2$ two-qubit unitary gates, acting on all the odd links in the first layer and all the even links in the second, as illustrated in Fig. 1. We set the initial state to be an infinite-temperature state $\rho(0) = \frac{1}{2^L} I$.

Throughout this work, we focus on a late-time state. We consider a total number of time steps that scale as $O(L)$ when analyzing the logarithmic purity [9,21,22] and $O(L^2)$ when analyzing the MBN. We find that MBN requires more time steps to saturate than logarithmic purity (see the behavior shown in Appendix B). The previous study [9] found that the purification phase transition is in the same universality class as MIPTs [1,2,23]. We are interested in how the purification (entanglement) phase transition is affected by the spatial nonuniformity of the measurement layer. We numerically investigate purification phase transitions by employing an efficient numerical algorithm for the stabilizer formalism [24,25] which can carry out large-scale numerical calculations. Technically, two-site random Clifford unitary gates are implemented by a lookup table scheme suggested in [19,20]. Moreover, in a pure initial state, the late-time state for the random Clifford circuit is related to the ground state obtained with an imaginary time evolution of an effective spin Hamiltonian [26]. Although it is obtained by approximating a circuit model, it allows us to make qualitative predictions about the late-time state. Based on the relation in [26], we derive that the circuit with the spatially modulated probability is related

to the imaginary time dynamics of the following disordered ZY spin model with random transverse field:

$$H_{\text{eff}} \equiv \sum_j \left(-\frac{2}{5}Z_jZ_{j+1} - \frac{1}{10}Y_jY_{j+1}\right) - \sum_j \left(\frac{2}{5} + 2\gamma_j\right)X_j. \tag{1}$$

A brief derivation of the effective Hamiltonian H_{eff} is shown in Appendix A, from which we find that $\gamma_j \propto p_j$. The late-time state of the circuit is related to the saturation state of the imaginary time evolution of the Hamiltonian,

$$\rho(t \to \infty) \approx \lim_{t\to\infty} e^{-tH_{\text{eff}}}|\rho_0\rangle\rangle, \tag{2}$$

where $|\rho_0\rangle\rangle$ represents a supervector state of $(\rho_0)^{\otimes 2}$. It consists of two copies of the initial density matrix. From this picture, the random transverse field in the Hamiltonian H_{eff} gives an impact on the criticality of the original Hamiltonian before the random transverse field is introduced. This influence resembles disordered quantum phase transitions, as discussed in [27,28]. From the viewpoints of the effective Hamiltonian and its ground states, we numerically investigate the late-time state.

III. TARGET PHYSICAL QUANTITIES

We explain the target physical quantities of this work. The first one is the logarithmic purity, denoted as S_P [9]:

$$S_P = -\log_2 \text{Tr}[\rho^2]. \tag{3}$$

This is also called the second-order Rényi entropy for the density matrix ρ [21,22]. The value is efficiently calculated in the stabilizer formalism [24,25]. Practically, it is calculated from the Gaussian elimination [17].

The second one is the MBN, defined as

$$\mathcal{E}_A \equiv \log_2 |\rho^{\Gamma_A}|_1,$$

where A is a half-chain subsystem, $|\cdot|_1$ represents the trace norm, and Γ_A is a partial transpose operation for the A subsystem. This quantity is a many-body version of the one for the few-spin system proposed in [14,15,29]. The negativity can reveal a transition of states by quantifying quantum entanglement in mixed states [16,17,30]. We explain the calculation of MBN [17,18,31,32] (the detailed derivation is described in Refs. [17,18]). As shown in Refs. [17,18,31,32], MBN is calculated with the following formula:

$$\mathcal{E}_A = \tfrac{1}{2}\text{rank}J,$$

where J is an $m \times m$ matrix, m is the total number of stabilizer generators for a state ρ, and here $m \leqslant L$. The matrix J is constructed using the anticommutation for truncated m stabilizer generators g_n^A $(n = 0, \ldots, m-1)$ of the state ρ. The truncated stabilizer generators are created as follows: We represent the stabilizer generators as a binary representation denoted by g_n [33]. Then, we truncate the binary representation vectors of each stabilizer generator to remove the elements of sites not in subsystem A as

$$g_n \longrightarrow g_n^A = \left(g_0^{n,x}, \ldots, g_k^{n,x} \middle| g_0^{n,z}, \ldots, g_k^{n,z}\right),$$

where $g_p^{n,x(z)} = 0$ or 1 and the binary components with the qubit label of subsystem A (here labeled by $0, \ldots, k$) remain.

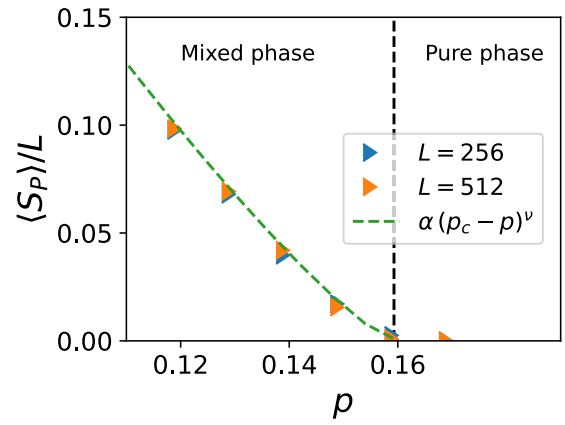


FIG. 2. Logarithmic purity with uniform measurement probability p, plotted as a function of p for various system sizes L. We took total time steps $t_{\text{step}} = 4L$. The green curve shows $\alpha(p_c - p)^\nu$ for $p \leqslant p_c = 0.159$ and $\nu = 1.22$.

Finally, by using the m truncated stabilizer generators g_n^A, we construct a matrix J, given by

$$(J)_{n,n'} = \begin{cases} 1 & \text{if } \{g_n^A, g_{n'}^A\} = 0, \\ 0 & \text{if } [g_n^A, g_{n'}^A] = 0, \end{cases}$$

where $\{g_n^A, g_{n'}^A\} = 0$ means that the truncated stabilizer generators g_n^A and $g_{n'}^A$ are anticommuting and $[g_n^A, g_{n'}^A] = 0$ means that the truncated stabilizer generators g_n^A and $g_{n'}^A$ are commuting. Thus, the matrix J is the binary $m \times m$ matrix. Finally, the calculation of the rank of J gives the value of MBN.

We consider the mean value of the physical quantities given by

$$\langle Q\rangle = \mathbb{E}[Q^s],$$

where $Q = S_P$ or $\mathcal{E}_A$, $\langle\cdot\rangle$ represents the mean value, and Q^s represents a single sample (labeled by s) of Q.

IV. NUMERICAL RESULTS

In this section, we show numerical results. In particular, we investigate late-time states that are almost saturated after $O(L)$ time steps for the logarithmic purity and after $O(L^2)$ time steps for MBN.

A. Case I: Uniform measurement probability p

We first show the uniform measurement probability case. That is, all sites on the measurement layer can be measured with a probability p, which is the same setup as in [9]. In Fig. 2, we show the logarithmic purity with uniform measurement probability p, plotted as a function of p for various system sizes L. We reproduced the same behavior of the logarithmic purity as in [9]. Two distinct phases appear for $p < 0.16$ and $p > 0.16$: mixed and pure phases, respectively. A purification phase transition exists between these phases. In the mixed phase for $p < 0.16$, we observed that $\langle S_P\rangle \approx L$, indicating a volume-law scaling. In contrast, in the pure phase for $p > 0.16$, $\langle S_P\rangle \approx 0$. Its behavior is independent of the system size, corresponding to the area-law scaling. These size scalings are the same as the volume-law and area-law phases

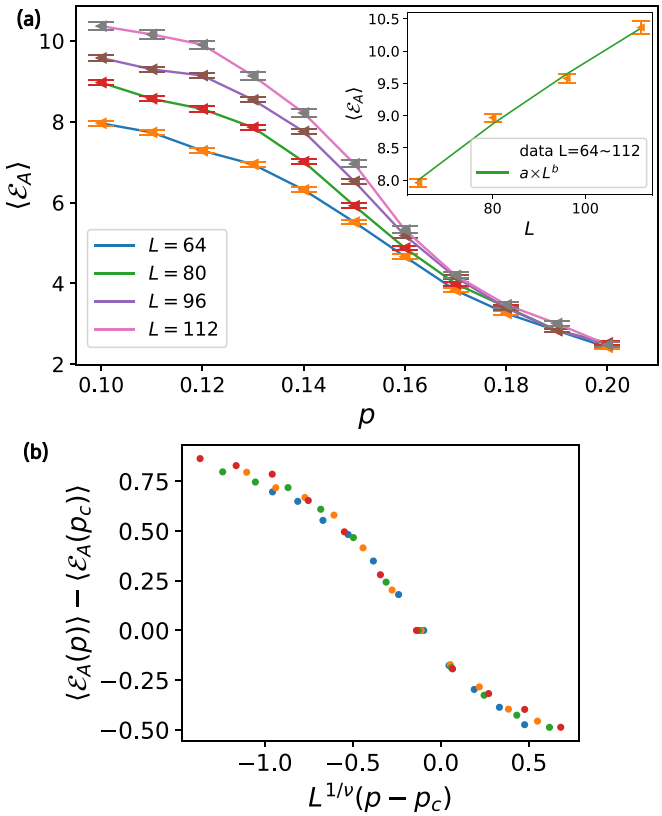


FIG. 3. (a) MBN with uniform measurement probability p, plotted as a function of p for various system sizes L. We took total time steps $t_{\text{step}} = L^2/4$. The inset represents the scaling behavior of MBN at a typical mixed phase $p = 0.10$, where the fitting function is set as $y = aL^b$ (green line) and we extracted $a \approx 1.18$ and $b \approx 0.460$. (b) Scaling data collapse for different system-size data for MBN. By using $L = 64$–112 data, we obtain $p_c = 0.167 \pm 0.00118$ and $\nu = 1.56 \pm 0.108$. We averaged $O(10^2)$ samples for each data point.

known in the study of MIPTs [1,2]. We employ the scaling form $\langle S_P \rangle / L \approx \alpha(p - p_c)^\nu$ (α is a constant) for $p < p_c$ to confirm the previous results, $p_c = 0.1593$ and $\nu = 1.28$, in [9]. We find $p_c = 0.159$ and $\nu = 1.22$. These values are almost the same as those in the previous study.

We next observe MBN, which is a main focus in this study. This quantity can extract quantum entanglement by partitioning the system into a mixed state. Numerical results for MBN as a function of p are displayed in Fig. 3(a). We observe a system-size dependence in $p < 0.17$. On the other hand, in $p > 0.17$, we observe area-law scaling [$\langle \mathcal{E}_A \rangle \approx O(L^0)$]. These numerical results suggest the presence of two different phases bordering on $p \approx 0.17$: An entanglement phase transition appears. We evaluated the system-size dependence of MBN at $p = 0.1$ using the scaling form $\langle \mathcal{E}_A(p = 0.1, L) \rangle = aL^b$ [see the inset of Fig. 3(a)]. We extracted $a \approx 1.18$ and $b \approx 0.460$.

Furthermore, we elucidate the phase transition point and its criticality in terms of MBN. Accordingly, we employ the following ansatz:

$$\langle \mathcal{E}_A(p) \rangle - \langle \mathcal{E}_A(p_c) \rangle = L^{\zeta/\nu} \tilde{f}(L^{1/\nu}(p - p_c)), \tag{4}$$

where p_c is the critical transition probability, ζ is a critical exponent, and ν is the correlation length critical exponent.

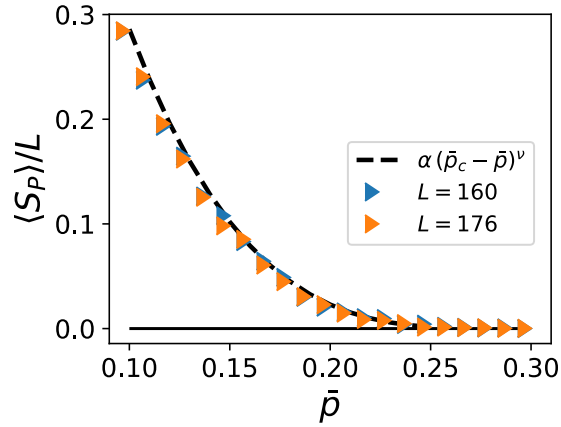


FIG. 4. Logarithmic purity with averaged probability $\bar{p}$, plotted as a function of $\bar{p}$ for various system sizes L. We took total time steps $t_{\text{step}} = 4L$. The dashed black curve shows $\alpha(\bar{p}_c - \bar{p})^\nu$ for $\bar{p} \leqslant \bar{p}_c = 0.290$ and $\nu = 3.38$. Each data point is calculated by using $O(10^2)$ samples.

Equation (4) is a more general ansatz than the one employed in [34] because of the presence of ζ. With the use of the Python package pyfssa [35,36], the finite-size scaling analysis is carried out. We obtain a clear data collapse, as shown in Fig. 3(b). We find $p_c = 0.167 \pm 0.00118$ and $\nu = 1.56 \pm 0.108$. The difference between the critical points p_c obtained from the logarithmic purity and the negativity is small, indicating that the two can be regarded as essentially identical in case I. This result is consistent with the expectation in Ref. [9] that the transition points coincide in systems with space-time symmetry (i.e., in the absence of quenched disorder). However, a noticeable difference appears in the correlation length critical exponent ν. This difference can be understood from Ref. [37]. It has been suggested that the critical exponent can vary depending on the choice of the observables.

B. Case II: Spatially modulated probability p

We next observe the spatially modulated probability case. The measurement probability is site dependent, with each site j having its own measurement probability p_j. The initial state, unitary layer, and total time steps (a typical time evolution is shown in Appendix B) are the same as those in case I.

In Fig. 4, we show the logarithmic purity, plotted as a function of the average measurement probability $\bar{p}$ for various system sizes L. A purification phase transition is also observed around $\bar{p} \approx 0.29$. Comparing Fig. 4 with Fig. 2, we can see a shift of the transition point $p_c = 0.159$ for case I to $\bar{p}_c = 0.290$ for case II. From the behavior of the logarithmic purity, we elucidate the transition by adopting the scaling form $\langle S_P \rangle / L \approx \alpha(\bar{p} - \bar{p}_c)^\nu$ with numerical results, where $\bar{p}_c$ and ν are the critical transition probability and the correlation length critical exponent from the point of view of the logarithmic purity. We evaluated $\bar{p}_c = 0.290$ and $\nu = 3.38$. These results are explicitly different from the uniform measurement probability (case I) [9].

We observe MBN for this spatially modulated probability case. In Fig. 5(a), MBN is plotted as a function of the averaged measurement probability $\bar{p}$ for various system sizes L. The

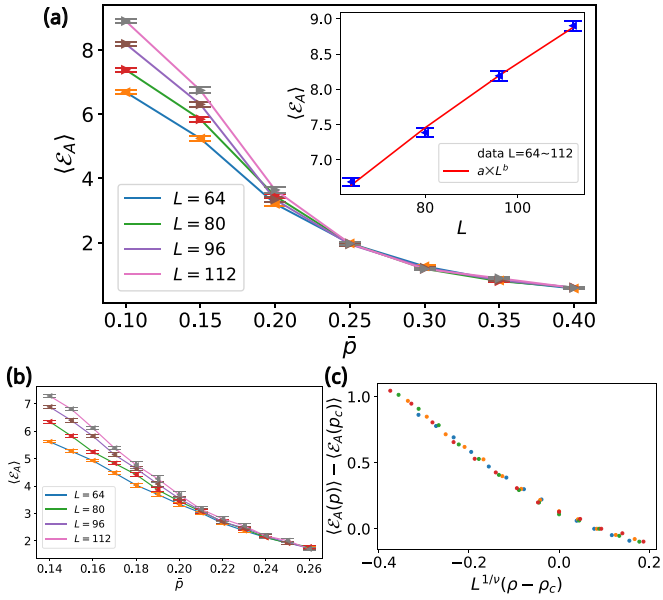


FIG. 5. (a) MBN with the averaged measurement probability, plotted as a function of $\bar{p}$ for various system sizes L. We took total time steps $t_{\text{step}} = L^2/4$. The inset represents the scaling behavior of MBN at a typical mixed phase $\bar{p} = 0.10$, where the red line is the fitting curve $y = aL^b$, with $a \approx 0.767$ and $b \approx 0.519$. (b) The details of the data for MBN around the purification phase transition point. (c) Scaling data collapse for different system-size data for MBN. By using $L = 64$–112 data, we obtain $\bar{p}_c = 0.220 \pm 0.00261$ and $\nu = 3.06 \pm 0.313$. We averaged $O(10^3)$ samples for each data point.

results indicate that MBN exhibits a system-size dependence for $\bar{p} < 0.20$. Additionally, it obeys the area law for $\bar{p} > 0.20$. These behaviors indicate the presence of two different phases: An entanglement phase transition appears. We also evaluate the system-size dependence of MBN at $\bar{p} = 0.1$ using the scaling form $\langle \mathcal{E}_A(\bar{p} = 0.1, L) \rangle = aL^b$. We extract $a \approx 0.767$ and $b \approx 0.519$. We estimate the phase transition point and its criticality in terms of MBN. We use the same finite-size scaling ansatz [4] as in case I. The finite-size scaling analysis indicates a clear data collapse, as shown in Fig. 5(c). We extract $\bar{p}_c = 0.220 \pm 0.00261$ and $\nu = 3.06 \pm 0.313$. A non-negligible difference in the critical point $\bar{p}_c$ was obtained between the logarithmic purity and the MBN. We comment here on the reason for this difference. In case II, the introduction of spatial modulation probability breaks the space-time symmetry that was preserved in case I. This breaking of space-time symmetry suggests that it could lead to the separation between the two transitions, as discussed in Ref. [9]. Each transition can be identified by the logarithmic purity and MBN. This difference in the two transition points we numerically observed indicates the occurrence of a separation between the purification phase transition and the entanglement transition.

V. COMPARISON AND DISCUSSION OF NUMERICAL RESULTS FOR CASE I AND CASE II

In this section, we focus on two main points. First, for both cases I and II, we discuss the result that MBN and logarithmic purity exhibit distinct power-law scaling behaviors with system size in the mixed phase. Second, the difference in the correlation length critical exponents between cases I and II can be understood in terms of the Harris criterion [13].

Regarding the first point, we performed a size scaling analysis of the MBN at measurement rate $p = 0.1$, assuming the fitting function $\langle \mathcal{E}_A(p = 0.1, L) \rangle = aL^b$. As a result, we numerically extracted the size exponent $b = 0.460$ for case I and $b = 0.519$ for case II. In contrast, the logarithmic purity $\langle S_P \rangle$ scaled as $\langle S_P \rangle / L \approx \alpha(p - p_c)^\nu$ for both cases I and II, indicating that $\langle S_P \rangle$ is proportional to the system size L. The behavior of $\langle S_P \rangle$ is different from that of MBN because b is less than 1 in both cases I and II. This is because MBN is able to capture only quantum correlations. According to [29], negativity can filter out such classical correlations in few-spin systems even though mixed states include classical correlations. We expect that MBN excludes classical correlations even in many-body settings. Furthermore, we compare our results with a previous study using MBN [16] in which a local dephasing was applied to the boundaries. In that setting, it is known that MBN scales as the $1/3$ power of the system size. That value is smaller than both of our calculated exponents, $b = 0.460$ and $b = 0.519$.

Regarding the second point, we explain the Harris criterion first. After that, we discuss our numerical results using the Harris criterion. For classical systems, Harris showed a phenomenological argument of the correlation length critical exponent ν [13], namely, the Harris criterion. The criterion is also applicable to quantum phase transitions in $(d + 1)$-dimensional space-time systems (where d is a spatial dimension) [27,38]. The Harris criterion in quantum phase transitions claims that the phase transition in systems without disorder is not affected by disorder if $\nu \geqslant 2/d$. This argument by Harris can also be interpreted as follows: If a quantum phase transition in a system without disorder with $\nu < 2/d$ exists, disorder can change the universality class of the phase transition. This interpretation and application of the Harris criterion are found in [39].

We discuss our numerical results based on the Harris criterion. The quantum circuits we consider are in one spatial dimension; hence, $d = 1$. In case I, we obtained correlation length critical exponents of $\nu = 1.22$ for S_P and $\nu = 1.56 \pm 0.108$ for $\mathcal{E}_A$. Remarkably, both ν are less than 2. According to the Harris criterion, for the quantum circuit model in case I, if a phase transition persists after perturbations are added, its universality class is expected to change. In fact, the values of ν we obtained for case II are $\nu = 3.38$ for S_P and $\nu = 3.06 \pm 0.313$ for $\mathcal{E}_A$. Both S_P and $\mathcal{E}_A$ of ν are different from case I. Therefore, case II maintains the purification phase transition and furthermore alters the universality class of quantum criticality. Our result obtained in the quantum circuit is in agreement with the Harris criterion.

VI. SPATIALLY MODULATED PROBABILITY FOR A RANDOM CLIFFORD UNITARY GATE

In this section, we investigate the effect of the spatial nonuniformity of a random Clifford unitary gate. This case also provides further insight into understanding the effects of spatial nonuniformity on the circuit.

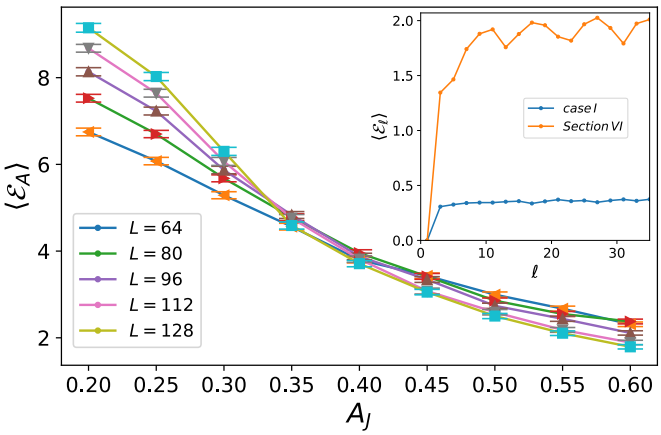


FIG. 6. A_J dependence of MBN for the late-time state at $t_{\text{step}} = L^2/4$. We averaged $O(10^3)$ samples for each data point. The inset represents the subsystem-size dependence of MBN at a mixed phase for $A_J = 0.6$, $p = 0.1$, and $L = 96$ (orange line). As a comparison, we plot a uniform probability ($p = 0.4$) case (case I), shown by the blue line.

We introduce the modulation for a two-site random Clifford unitary gate for each nearest-neighbor site. Here, we consider a spatially modulated probability p_j^u (j is the link between the jth and $(j+1)$th sites) defined by the following formula:

$$p_j^u = \frac{1 + A_J \cos(2\pi Q j)}{1 + A_J}, \tag{5}$$

where $0 \leqslant A_J \leqslant 1$ and $Q = \frac{1+\sqrt{5}}{2}$ (the golden ratio). We then fix the uniform measurement probability at $p = 0.1$ for the measurement layer.

In the effective Hamiltonian picture, the effect of p_j^u can be regarded as spatially modulated couplings in the ZY term. The effective Hamiltonian is

$$H_{\text{eff}} \equiv \sum_j \tilde{J}_j \left(-\frac{2}{5} Z_j Z_{j+1} - \frac{1}{10} Y_j Y_{j+1} \right) + \sum_j \left(-\frac{2}{5} - 2\gamma_0 \right) X_j, \tag{6}$$

where $\tilde{J}_j \propto p_j^u$ and $\gamma_0 \propto p = 0.1$. This spatial modulation acts like a quasiperiodic ferromagnetic ZY coupling. As A_J gets large, entanglement generation is suppressed due to the reduced probability of unitary gate application. From the effective Hamiltonian picture, we expect that even in the circuit system, the effects of the modulation lead to a change in the mixed-state dynamics and its late-time state and there is a critical A_J (p_j^u) required to change the entanglement structure.

In this setting of unitary gates, we numerically observe the MBN of the late-time state as varying A_J. The results are shown in Fig. 6. A data crossing appears at $A_J \approx 0.35$. This data crossing implies the presence of a phase transition. In the region where $A_J < 0.35$, an entanglement phase is observed in which the value of MBN increases as the system size increases. In contrast, for $A_J > 0.35$, MBN exhibits a tiny decrease as the system size increases. Hereafter, for convenience, we refer to the regime of $A_J > 0.35$ as the area-law-like phase. This phase is different from the pure phase in both cases I and II in the previous section, where MBN exhibits system-size independence (area-law scaling).

In the inset of Fig. 6, to elucidate the entanglement structure and its difference from that of the previous area-law phases in case I and case II, we observe the subsystem-size dependence of MBN, with the subsystem size denoted by ℓ. The MBN is given by $\mathcal{E}_\ell \equiv \log_2 |\rho^{\Gamma_\ell}|_1$. The mean value of $\mathcal{E}_\ell$, denoted as $\langle \mathcal{E}_\ell \rangle$, is obtained by averaging over different samples. The orange line in the inset of Fig. 6 represents $\langle \mathcal{E}_\ell \rangle$ in the area-law-like phase regime, with parameters $A_J = 0.6$, $p = 0.1$, and $L = 96$. We show the subsystem-size dependence of MBN in the pure phase with $p = 0.4$ in case I as a comparison, the result of which is the blue line in the inset of Fig. 6. The result indicates that MBN for the quasiperiodic unitary case is larger than that of case I. It implies the area-law-like phase exhibits short-range entanglement. Then, we observe an oscillating behavior of MBN in this model with varying ℓ; the period of oscillation corresponds to the period of the quasiperiodic modulation probability. This indicates that the subsystem-size dependence of the entanglement is strongly affected by the quasiperiodic modulation of the two-site unitary gate.

VII. CONCLUSIONS

We numerically investigated the effect of spatial modulation in a random Clifford circuit and its mixed-state dynamics by focusing on MBN. While we employed the same quenched spatial randomness as in Ref. [10], we focused on the case of mixed states, which differs from that in Ref. [10]. Furthermore, the observables are also different from those used in Ref. [10]. For these reasons, we cannot assert that our results completely coincide with the results reported in Ref. [10]. As demonstrated by our numerical results, we found that MBN is valid to extract internal quantum entanglement for mixed states and numerically demonstrated that MBN is a good indicator to characterize the purification phase transition and to detect its criticality, especially the correlation length critical exponent ν and critical measurement probability p_c. In case I, we found $p_c = 0.167 \pm 0.00118$ and $\nu = 1.56 \pm 0.108$. On the other hand, in case II, we found that the spatially modulated probability gives significant effects on the criticality of the purification phase transition as $\bar{p}_c = 0.220 \pm 0.00261$ and $\nu = 3.06 \pm 0.313$. The main result of our study is that MBN captures the changes in the correlation length critical exponent ν in cases I and II. This change in the quantum criticality is understood by using the Harris criterion. In case I, the correlation length critical exponent satisfies $\nu = 1.22 < 2$ for S_P and $\nu = 1.56 \pm 0.108 < 2$ for $\mathcal{E}_A$ (where $d = 1$). Through the Harris criterion, disorder changes the universality class of the phase transition. In fact, in case II, the correlation length critical exponent in both the logarithmic purity and MBN differs from that in case I, suggesting a distinct universality class. These results are summarized in the Table I.

We conclude that the change in the correlation length critical exponent is consistent with the insight discussed in Sec. II [Eq. (1)], namely, that the random transverse field affects quantum criticality. The numerical results obtained from the logarithmic purity and the MBN suggest that the

TABLE I. Numerically extracted correlation length critical exponents in cases I and II. In this work, we estimated the correlation length critical exponent ν from the MBN in cases I and II, as well as from the logarithmic purity in case II.

	Logarithmic purity	MBN
Case I	$\nu = 1.22$	$\nu = 1.56 \pm 0.108$
Case II	$\nu = 3.38$	$\nu = 3.06 \pm 0.313$

transition points are separated due to the spatial modulation. We comment on the order of entanglement and purification phase transition. In our results, the critical probability of the entanglement phase transition ($\bar{p}_c = 0.220$) is smaller than that of the purification one ($\bar{p}_c = 0.290$). Qualitatively, this is because the quantum correlation captured by the MBN is spatially extended in a one-dimensional system. Even if a measurement is performed at any single point within the entangled region, the correlation is immediately destroyed. On the other hand, the purification phase transition requires that measurements are applied to all sites to make the purity almost zero. This qualitative difference leads to the order of the transitions. Moreover, in a previous study [10], the entanglement phase transition was studied using the tripartite mutual information and the transition point was estimated to be $\bar{p}_c = 0.145$ [10]. This value is smaller than that of our entanglement phase transition. The tripartite mutual information involves a more complex combination of correlations and is defined over a spatially extended structure. Therefore, it is expected to decay more strongly with single-local measurements compared to MBN. Consequently, a critical value smaller than the transition point we obtained was reported.

We also obtained another important numerical result regarding the correlation length critical exponent ν. Although a certain difference was observed in ν, both results satisfy the Harris criterion, indicating the validity of our study.

A previous study [10] discussed that a Griffith regime can emerge in pure-state dynamics with quenched spatial randomness. Based on our numerical results, whether Griffith's effects appear in the mixed-state dynamics remains inconclusive. The numerical analysis of the mixed-state dynamics using the MBN does not have sufficient resolution to capture such a subtle regime. However, we do not rule out the existence. The Griffith regime could be around the entanglement phase transition characterized by the MBN since, in Ref. [10], the calculation was performed using the entanglement entropy, which characterizes the slow dynamics associated with entanglement, i.e., the spatial correlations in the system. On the other hand, the purification phase transition observed through the logarithmic purity reflects correlations across different times in the system. It remains an open question whether the Griffith effect also affects such temporal correlations and induces a similar critical behavior in mixed-state dynamics.

Moreover, we numerically investigated the effect of introducing a quasiperiodic spatially modulated probability for random Clifford unitary gates. This modulation also induces a purification phase transition, but the area-law-like phase appears to differ from the pure phase in cases I and II in terms of the subsystem dependence of MBN. This indicates that a unique internal correlation pattern appears in the area-law-like phase. According to [28,40], quasiperiodic modulation induces a quantum phase transition. Therefore, the difference between the area-law-like phase and the area-law phase can be understood as the difference in the localized phase.

Apart from numerical analysis of the circuit, some master equations can describe the circuit dynamics [41]. Understanding measurement-induced (purification) phase transitions from the theoretical framework of the master equations and further investigating the relationship between the numerical results and these equations are an interesting future subject.

ACKNOWLEDGMENT

This research was supported in part by JSPS KAKENHI Grants No. JP24K06878, No. JP24K00563, No. JP24K02948, and No. JP21H04446 and CSIS at Tohoku University.

DATA AVAILABILITY

The data that support the findings of this article are not publicly available upon publication because it is not technically feasible and/or the cost of preparing, depositing, and hosting the data would be prohibitive within the terms of this research project. The data are available from the authors upon reasonable request.

APPENDIX A: EFFECTIVE SPIN MODEL

In this appendix, we briefly show the derivation of the effective Hamiltonian in the main text [Eq. (1)] by reviewing the analytical manipulations in Refs. [4–7]. We show that the dynamics of a hybrid random quantum circuit can be related to an imaginary time dynamics with an effective quantum spin model.

As a circuit related to the one in the main text (shown in Fig. 1), we consider the Haar random circuit shown in Fig. 7, where the small time interval includes a local layer of an on-site Haar random unitary applied to every site, a two-site random unitary layer including the even site pair, a two-site random unitary layer including the odd site pair, and two measurement layers. In the measurement layer, we consider that each site is measured with a spatially modulated probability p_i, which is the only difference from the original setup [4,5,7]. The schematic of the small time interval is shown in Fig. 7.

We start with two copies of a density matrix labeled by s, $(\rho_s)^{\otimes 2}$. Here, we introduce the supervector representation $(\rho_s)^{\otimes 2} \longrightarrow |\rho_s\rangle\rangle$ [7]. Then, the average density matrix over samples (labeled by s) is given by [5]

$$|\rho\rangle\rangle \equiv \sum_s |\rho_s\rangle\rangle. \tag{A1}$$

Note that this vector is un-normalized (the norm is related to the purity of the system). We expect that the average late-time state for $|\rho\rangle\rangle$ gives qualitative insight into the late-time state of the Clifford circuit in the main text.

Based on the average picture, we start to consider the evolution of the small time interval δt. The operation is

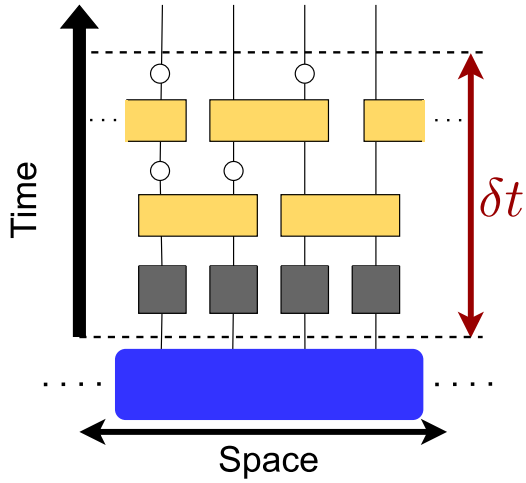


FIG. 7. Hybrid (Haar) random circuit. The yellow blocks represent two-site Haar random unitary gates, the gray blocks represent single-site Haar random unitary gates, and the small white circles represent projective measurements with the on-site Z_j measurement operator, where the measurement rate is site-dependent p_i. This model can be qualitatively related to the circuit model in the main text (shown in Fig. 1).

given by [5]

$$\begin{aligned}&|\rho(t+\delta t)\rangle\rangle\\&=(MU_{NN_o}MU_{NN_e})U_1|\rho(t)\rangle\rangle\\&=(PMP)(PU_{NN_o}P)(PMP)(PU_{NN_e}P)|\rho(t)\rangle\rangle,\end{aligned}\tag{A2}$$

where U_1 is a layer constituted by the product of single-site Haar random unitaries (the black squares in Fig. 7), $U_{NN_{e(o)}}$ represents a unitary layer constituted by two-site Haar random unitaries for even (odd) links, and P is the average single-qubit Haar random gate, which can be represented by an effective spin-1/2 Hilbert space [5],

$$P\equiv\bigotimes_{j=0}^{L-1}\sum_{\sigma=\uparrow,\downarrow}|\sigma\rangle\rangle\langle\langle\sigma|_j.\tag{A3}$$

Here, $\{|\uparrow\rangle\rangle_j,|\downarrow\rangle\rangle_j\}$ can be regarded as a spin-1/2 orthogonal basis on a two-dimensional Hilbert space on site j, and P acts as a projector [7].

Based on the projector P and employing the transfer matrix picture [7], the average action of the two-site Haar random gate can be described in terms of the effective spin-1/2 bases as

$$PU_{NN_e}P\equiv\prod_{\ell=0}^{L/2}[I+\delta tP\overline{u_{2\ell,2\ell+1}}P].\tag{A4}$$

By considering an exponent form for the above equation, we can define a local effective Hamiltonian:

$$\mathcal{P}U_{NN}\mathcal{P}\equiv e^{-\delta t\sum_j h_{NN}^{j,j+1}}.\tag{A5}$$

Here, we omitted the even or odd label of the unitary gates ($U_{NN_{e(o)}}\to U_{NN}$).

We next describe the concrete form of $h_{NN}^{j,j+1}$. The local average two-site Haar random gate is given by [7]

$$\begin{aligned}\overline{u_{j,j+1}}&=\overline{(U_{j,j+1}\times U_{j,j+1}^*)^{\otimes 2}}\\&=\tfrac{1}{15}|\mathcal{I}_j\mathcal{I}_{j+1}\rangle\rangle\langle\langle\mathcal{I}_j\mathcal{I}_{j+1}|+\tfrac{1}{15}|\mathcal{C}_j\mathcal{C}_{j+1}\rangle\rangle\langle\langle\mathcal{C}_j\mathcal{C}_{j+1}|\\&\quad-\tfrac{1}{60}|\mathcal{I}_j\mathcal{I}_{j+1}\rangle\rangle\langle\langle\mathcal{C}_j\mathcal{C}_{j+1}|\\&\quad-\tfrac{1}{60}|\mathcal{C}_j\mathcal{C}_{j+1}\rangle\rangle\langle\langle\mathcal{I}_j\mathcal{I}_{j+1}|,\end{aligned}\tag{A6}$$

where

$$|\mathcal{I}_j\rangle\rangle=c_+|\uparrow\rangle\rangle_j+c_-|\downarrow\rangle\rangle_j,\tag{A7}$$

$$|\mathcal{C}_j\rangle\rangle=c_-|\uparrow\rangle\rangle_j+c_+|\downarrow\rangle\rangle_j,\tag{A8}$$

with $c_\pm=(\sqrt{3}\pm1)/(\sqrt{2})$.

If we use (A4), (A5), (A6), (A7), and (A8), $h_{NN}^{j,j+1}$ is given by

$$h_{NN}^{j,j+1}=\sum_{\alpha,\beta,\gamma,\lambda=\uparrow,\downarrow}C_{\gamma,\lambda}^{\alpha,\beta}|\alpha\beta\rangle\rangle_{j,j+1}\langle\langle\gamma\lambda|_{j,j+1},\tag{A9}$$

$$C_{\gamma,\lambda}^{\alpha,\beta}={}_{j,j+1}\langle\langle\alpha\beta|\overline{u_{j,j+1}}|\gamma\lambda\rangle\rangle_{j,j+1}.\tag{A10}$$

If we represent the 4×4 matrix $C_{\gamma,\lambda}^{\alpha,\beta}$ in terms of two Pauli matrix products, $h_{NN}^{j,j+1}$ becomes

$$h_{NN}^{j,j+1}=-\tfrac{2}{5}Z_jZ_{j+1}-\tfrac{1}{10}Y_jY_{j+1}+\tfrac{1}{5}(X_j+X_j+1).\tag{A11}$$

Here, we dropped a constant identity.

Furthermore, we use the same procedure for the measurement layer (PMP). The operator M [5] is given as

$$\begin{aligned}&M\equiv\prod_j M_j,\\&M_j=(1-p_j)\mathbf{1}^{\otimes4}+p_j\sum_{\mu=\pm}P_{j,\mu}^{\otimes4},\quad P_{j,\mu}=\frac{1+\mu\sigma_j^z}{2}.\end{aligned}$$

Then, the measurement layer (PMP) can be exponetiated as [5]

$$\begin{aligned}&(PMP)\equiv e^{-\delta t\sum_j h_j^m},\\&h_j^m=\frac{\gamma_j}{3}X_j+\left(\frac{1}{3}-\gamma_j\right)I_j,\end{aligned}\tag{A12}$$

where we set $p_j=\gamma_j\delta t$ and the term h_j^m is a *spatially modulated local transverse field*. The final identity term in h_j^m can be dropped. Consequently, from the form of the local Hamiltonian $h_{NN}^{j,j+1}$ and spatially modulated local transverse field h_j^m, the average operation within the small time interval is approximately given by

$$\begin{aligned}&(PMP)(PU_{NN_o}P)(PMP)(PU_{NN_e}P)\approx e^{-\delta tH_{\rm eff}},\\&H_{\rm eff}\equiv\sum_j\left(-\frac{2}{5}Z_jZ_{j+1}-\frac{1}{10}Y_jY_{j+1}\right)\\&\quad+\sum_j\left(-\frac{2}{5}-2\gamma_j\right)X_j.\end{aligned}\tag{A13}$$

The model is a modified ZY model with a random transverse field. The effective Hamiltonian $H_{\rm eff}$ can give many

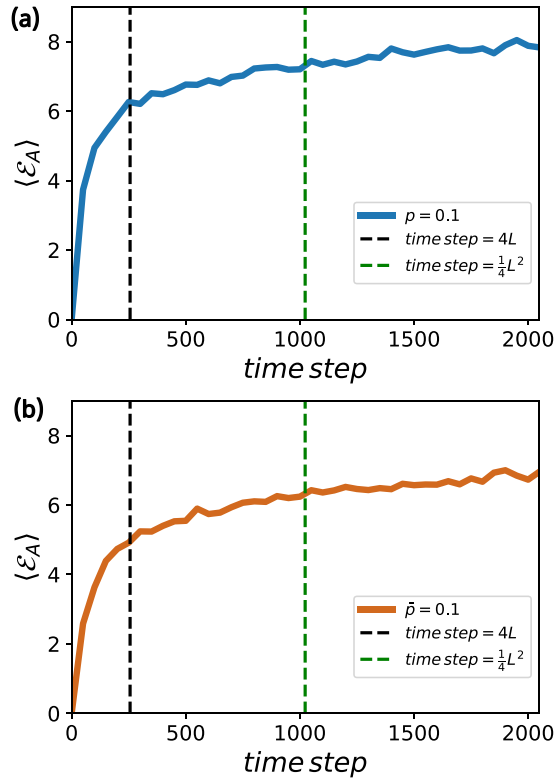


FIG. 8. Typical time evolution behaviors of MBN for (a) uniform probability case I and (b) spatially modulated probability case II.

insights into the late-time state for the circuit considered in the main text.

If we accumulate the evolution operator of the small time interval, the imaginary time dynamics induced by H_{eff} is given by

$$|\rho(t)\rangle\rangle = e^{-tH_{\text{eff}}}|\rho(0)\rangle\rangle. \tag{A14}$$

We set the initial supervector $|\rho(0)\rangle\rangle = \prod_j |\mathcal{I}_j\rangle\rangle$, corresponding to the infinite-temperature state $\frac{1}{2^L}I$.

In many cases, the imaginary time dynamics leads to a ground state of the Hamiltonian of H_{eff},

$$\lim_{t\to\infty} |\rho(t)\rangle\rangle = |\text{GS}\rangle\rangle,$$

where $|\text{GS}\rangle$ is a ground state of the Hamiltonian H_{eff}. This ground state gives qualitative insight into the late-time state in the Clifford circuit considered in the main text.

APPENDIX B: TIME EVOLUTION AND SATURATION BEHAVIOR OF MBN

In this appendix, we show typical time evolution and observe saturation behaviors of MBN for both the uniform and spatially modulated probability cases, where we set $p = 0.1$ and $\bar{p} = 0.1$. The numerical results are displayed in Fig. 8. These results indicate that taking the time step $O(L^2)$ is sufficient to get nearly steady states, while $O(L)$ time steps may not. We expect that this tendency is true for different p or $\bar{p}$, except for the critical transition points. In addition, by taking into account the limit of our numerical resources, we observe a late-time state at $t_{\text{step}} = L^2/4$ in most of the numerical calculations in this work.

[1] Y. Li, X. Chen, and M. P. A. Fisher, Measurement-driven entanglement transition in hybrid quantum circuits, Phys. Rev. B **100**, 134306 (2019).
[2] B. Skinner, J. Ruhman, and A. Nahum, Measurement-induced phase transitions in the dynamics of entanglement, Phys. Rev. X **9**, 031009 (2019).
[3] M. P. Fisher, V. Khemani, A. Nahum, and S. Vijay, Random quantum circuits, Annu. Rev. Condens. Matter Phys. **14**, 335 (2023).
[4] Y. Bao, S. Choi, and E. Altman, Symmetry enriched phases of quantum circuits, Ann. Phys. (Amsterdam, Neth.) **435**, 168618 (2021).
[5] M. Block, Y. Bao, S. Choi, E. Altman, and N. Y. Yao, Measurement-induced transition in long-range interacting quantum circuits, Phys. Rev. Lett. **128**, 010604 (2022).
[6] B. C. Dias, D. Perković, M. Haque, P. Ribeiro, and P. A. McClarty, Quantum noise as a symmetry-breaking field, Phys. Rev. B **108**, L060302 (2023).
[7] Y. Bao, M. Block, and E. Altman, Finite-time teleportation phase transition in random quantum circuits, Phys. Rev. Lett. **132**, 030401 (2024).
[8] Y. Li and M. P. A. Fisher, Statistical mechanics of quantum error correcting codes, Phys. Rev. B **103**, 104306 (2021).
[9] M. J. Gullans and D. A. Huse, Dynamical purification phase transition induced by quantum measurements, Phys. Rev. X **10**, 041020 (2020).
[10] A. Zabalo, J. H. Wilson, M. J. Gullans, R. Vasseur, S. Gopalakrishnan, D. A. Huse, and J. H. Pixley, Infinite-randomness criticality in monitored quantum dynamics with static disorder, Phys. Rev. B **107**, L220204 (2023).
[11] G. Shkolnik, A. Zabalo, R. Vasseur, D. A. Huse, J. H. Pixley, and S. Gazit, Measurement induced criticality in quasiperiodic modulated random hybrid circuits, Phys. Rev. B **108**, 184204 (2023).
[12] H. Ha, A. Pandey, S. Gopalakrishnan, and D. A. Huse, Measurement-induced phase transitions in systems with diffusive dynamics, Phys. Rev. B **110**, L140301 (2024).
[13] A. B. Harris, Effect of random defects on the critical behavior of Ising models, J. Phys. C **7**, 1671 (1974).
[14] A. Peres, Separability criterion for density matrices, Phys. Rev. Lett. **77**, 1413 (1996).
[15] R. Horodecki, P. Horodecki, M. Horodecki, and K. Horodecki, Quantum entanglement, Rev. Mod. Phys. **81**, 865 (2009).
[16] Z. Weinstein, Y. Bao, and E. Altman, Measurement-induced power-law negativity in an open monitored quantum circuit, Phys. Rev. Lett. **129**, 080501 (2022).

[17] S. Sang, Y. Li, T. Zhou, X. Chen, T. H. Hsieh, and M. P. A. Fisher, Entanglement negativity at measurement-induced criticality, PRX Quantum **2**, 030313 (2021).
[18] B. Shi, X. Dai, and Y.-M. Lu, Entanglement negativity at the critical point of measurement-driven transition, arXiv:2012.00040.
[19] R. Koenig and J. A. Smolin, How to efficiently select an arbitrary Clifford group element, J. Math. Phys. **55**, 122202 (2014).
[20] J. Richter, O. Lunt, and A. Pal, Transport and entanglement growth in long-range random Clifford circuits, Phys. Rev. Res. **5**, L012031 (2023).
[21] Y. Ashida, S. Furukawa, and M. Oshikawa, System-environment entanglement phase transitions, Phys. Rev. B **110**, 094404 (2024).
[22] Y. Zou, S. Sang, and T. H. Hsieh, Channeling quantum criticality, Phys. Rev. Lett. **130**, 250403 (2023).
[23] Y. Li, X. Chen, A. W. W. Ludwig, and M. P. A. Fisher, Conformal invariance and quantum nonlocality in critical hybrid circuits, Phys. Rev. B **104**, 104305 (2021).
[24] D. Gottesman, The Heisenberg representation of quantum computers, arXiv:quant-ph/9807006.
[25] S. Aaronson and D. Gottesman, Improved simulation of stabilizer circuits, Phys. Rev. A **70**, 052328 (2004).
[26] Y. Bao, S. Choi, and E. Altman, Theory of the phase transition in random unitary circuits with measurements, Phys. Rev. B **101**, 104301 (2020).
[27] S. Sachdev, *Quantum Phase Transitions* (Cambridge University Press, Cambridge, 2011).
[28] A. Chandran and C. R. Laumann, Localization and symmetry breaking in the quantum quasiperiodic Ising glass, Phys. Rev. X **7**, 031061 (2017).
[29] M. B. Plenio, Logarithmic negativity: A full entanglement monotone that is not convex, Phys. Rev. Lett. **95**, 090503 (2005).
[30] T.-C. Lu, T. H. Hsieh, and T. Grover, Detecting topological order at finite temperature using entanglement negativity, Phys. Rev. Lett. **125**, 116801 (2020).
[31] S. Sharma, X. Turkeshi, R. Fazio, and M. Dalmonte, Measurement-induced criticality in extended and long-range unitary circuits, SciPost Phys. Core **5**, 023 (2022).
[32] Y. Kuno, T. Orito, and I. Ichinose, Phase transition and evidence of fast-scrambling phase in measurement-only quantum circuits, Phys. Rev. B **108**, 094104 (2023).
[33] M. A. Nielsen and I. L. Chuang, *Quantum Computation and Quantum Information*, 10th ed. (Cambridge University Press, New York, 2011).
[34] Z. Weinstein, Efficient detection of strong-to-weak spontaneous symmetry breaking via the Rényi-1 correlator, Phys. Rev. Lett. **134**, 150405 (2025).
[35] O. Melchert, Autoscale.Py - a program for automatic finite-size scaling analyses: A user's guide, arXiv:0910.5403.
[36] A. Sorge, Autoscale.Py - a program for automatic finite-size scaling analyses: A user's guide, Zenodo (2015), doi: https://zenodo.org/records/35293.
[37] A. Zabalo, M. J. Gullans, J. H. Wilson, S. Gopalakrishnan, D. A. Huse, and J. H. Pixley, Critical properties of the measurement-induced transition in random quantum circuits, Phys. Rev. B **101**, 060301(R) (2020).
[38] J. T. Chayes, L. Chayes, D. S. Fisher, and T. Spencer, Finite-size scaling and correlation lengths for disordered systems, Phys. Rev. Lett. **57**, 2999 (1986).
[39] J.-H. Peng, L.-W. Huang, D.-R. Tan, and F.-J. Jiang, Validity of the Harris criterion for two-dimensional quantum spin systems with quenched disorder, Phys. Rev. B **101**, 174404 (2020).
[40] K. Ohgane, Y. Masaki, and H. Matsueda, Quasiparticle dynamics in a quasiperiodic Ising model with temporally fluctuating transverse fields, Phys. Rev. B **107**, 134201 (2023).
[41] Y.-N. Zhou, Generalized Lindblad master equation for measurement-induced phase transition, SciPost Phys. Core **6**, 023 (2023).